

## BAR-HALO FRICTION IN GALAXIES I: SCALING LAWS

J. A. SELLWOOD

Rutgers University, Department of Physics & Astronomy,  
 136 Frelinghuysen Road, Piscataway, NJ 08854-8019  
*sellwood@physics.rutgers.edu*

*Revised version submitted to ApJ*

### ABSTRACT

It has been known for some time that rotating bars in galaxies experience dynamical friction against the halo. However, recent attempts to use this process to place constraints on the dark matter density in galaxies and possibly also to drive dark matter out of the center have been challenged. This paper uses simplified numerical experiments to clarify the friction process and confirm some theoretical results. It also demonstrates that bar slow down should be captured correctly in simulations having modest spatial resolution and practicable numbers of particles. Angular momentum lost from a realistic bar does not cause significant evolution of the halo density profile. Subsequent papers in this series delineate the dark matter density that can be tolerated in halos of different density profiles.

*Subject headings:* galaxies: formation — galaxies: kinematics and dynamics — galaxies: halos — dark matter

### 1. INTRODUCTION

Friction between a rotating bar and a massive halo was first reported many years ago (Sellwood 1980) and has subsequently been worked on sporadically (Tremaine & Weinberg 1984; Weinberg 1985; Hernquist & Weinberg 1992; Athanassoula 1996). It has, however, received a lot of attention in recent years as a potential probe of, and structuring mechanism for, dark matter halos. Debattista & Sellwood (1998, 2000) argued that the fact that bars appear not to have been slowed places an upper bound on the density of the dark matter halo in barred disk galaxies. Weinberg & Katz (2002) argue that the transfer of angular momentum from the bar to the halo could reduce the central density of the dark matter halo by a substantial factor.

Both of these claims have subsequently been disputed; Valenzuela & Klypin (2003) claim a counter-example of a bar that does not experience much friction and Athanassoula (2003) points out that the velocity dispersions of halos and disks are relevant factors. In addition, Sellwood (2003) found that contraction of the disk mass distribution as it lost angular momentum to the halo dragged halo mass in with it, causing the density density to rise, rather than to decrease. Valenzuela & Klypin (2003) and Holley-Bockelmann, Weinberg & Katz (2003) blame discrepant conclusions on inadequacies of respectively the codes and the number of particles employed, but it is more likely that the different results reported by these authors arise mainly because the physical models differ. There have been a few tests with different codes from the same initial conditions and the results compare quite well (*e.g.* O'Neill & Dubinski 2003; Sellwood 2003); other comparisons are reported here and in Paper II (Sellwood & Debattista, in preparation).

The present paper attempts to clarify the physics of dynamical friction between a bar and a halo and to show that it can be correctly reproduced in simulations of a size that is readily accessible with current computational resources. The halo density profile is hardly changed in most simulations presented here, but I do find that huge bars with unrealistic stores of angular momentum can cause the central

density to decrease. The constraint on halo density that can be deduced from the existence of strong, fast bars and the results reported by Valenzuela & Klypin (2003) and by Athanassoula (2003) will be addressed in Paper II.

### 2. THEORETICAL BACKGROUND

Dynamical friction (Chandrasekhar 1943) is the retarding force experienced by a massive perturber moving through a background of low-mass particles. It arises, even in a perfectly collisionless system, from the vector sum of the impulses the perturber receives from the particles as they are deflected by its gravitational field. The friction force can also be viewed, equivalently, as the gravitational attraction on the perturber of the density excess, or wake, that develops behind it as it moves, as was nicely illustrated by Mulder (1983).

Chandrasekhar's formula (eq. 7-17 of Binney & Tremaine 1987; hereafter BT) for the acceleration  $a_M$  of a perturber of mass  $M$  moving at speed  $v_M$  through a uniform background, density  $\rho$ , of non-interacting particles having an isotropic velocity distribution with a 1-D rms velocity spread  $\sigma$ , may be written as

$$a_M(v_M) = 4\pi \ln \Lambda G^2 \frac{M\rho}{\sigma^2} V\left(\frac{v_M}{\sigma}\right). \quad (1)$$

Here,  $\Lambda$  ( $= b_{\max}/b_{\min}$ ) is the argument of the usual Coulomb logarithm, and the dimensionless function  $V$  is drawn in Figure 1 for a Gaussian distribution of velocities; other velocity distributions would yield a different functional form.

The simplifying assumptions in its derivation strictly invalidate application of equation (1) to the physically more interesting problem of friction in a non-uniform medium in which the background particles are confined by a potential well and interact with the perturber repeatedly. Repeated encounters between the perturber and the background particles require a more sophisticated treatment.

Tremaine & Weinberg (1984, hereafter TW84) developed the basic theory of dynamical friction by a generic perturber in spherical systems. Following the precepts set

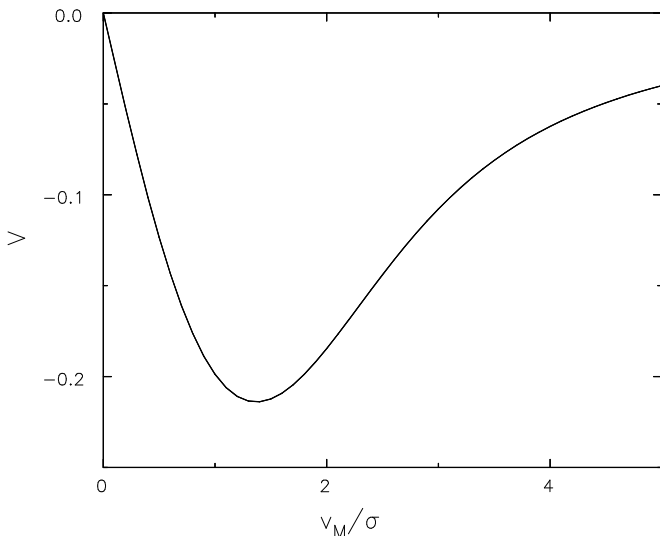


FIG. 1.— The dimensionless acceleration function  $V$  defined in equation (1) for the case of a Gaussian distribution of velocities among the background particles.

out in Lynden-Bell & Kalnajs (1972), they derived an expression for the “LBK torque” in a spherical system, which they showed arises purely at resonances. Weinberg (1985) gave a specific evaluation of the LBK torque for the case of a bar.

The daunting expression for the LBK torque given by TW84 (their eq. 65) does not appear to resemble eq. (1) above. However, TW84 also reformulate the original Chandrasekhar problem in a manner that highlights the similarities with the LBK torque in a spherical system, but which contains no resonant terms because the system is infinite. A naïve guess, therefore, is that the LBK torque causes the angular acceleration of the perturber to scale as

$$\dot{\Omega}_p \propto \frac{M_p \rho_s}{\sigma_s^2} \Theta \left( \frac{\Omega_p a}{\sigma_s} \right), \quad (2)$$

where  $M_p$  and  $\Omega_p$  are the mass and instantaneous angular speeds of the perturber,  $\rho_s$  and  $\sigma_s$  are the characteristic density and velocity dispersion of the spherical system, and the dimensionless function  $\Theta$  contains all the complicated dependence on the details of the distribution function, potential well, resonances, bar shape, *etc.* A characteristic length scale  $a$  is included in order to make the argument of  $\Theta$  dimensionless. The functions  $\Theta(x)$  and  $V(x)$  share the general properties that they are negative, at least for isotropic distribution functions (TW84), they must  $\rightarrow 0$  as  $x \rightarrow \infty$ , and that they can reasonably be expected to be  $\propto x$  as  $x \rightarrow 0$ .

Because resonances can produce non-linear orbital responses from quite mild potential perturbations, TW84 examined the resonant terms more carefully. They showed that the LBK torque formula remains valid provided the bar pattern speed changes sufficiently rapidly that particles make a “fast” passage through the resonance. By this, they mean that the pattern speed of the bar is changing sufficiently rapidly that “large non-linear resonant perturbations do not have time to develop before the star has crossed the resonance.” The possible trapping of orbits by

bars was discussed by Lynden-Bell (1979) in the analogous case of disks; he separated the motion of a star into a fast component around an ellipse and a slow angular frequency of libration of the ellipse in the resonant potential. Since the libration period is generally rather long, TW84 and Weinberg (1985) argued that fast passage through the resonance is the correct assumption, and their LBK torque formula should be valid.

The role of resonances has been re-emphasized in recent work (Weinberg & Katz 2002; Athanassoula 2003; Holley-Bockelmann, *et al.* 2003). Yet all this emphasis on resonances may have obscured the fact that friction can equivalently be regarded as the gravitational coupling between the bar and the misaligned density response in the halo. A detailed dynamical understanding of the origin of the misalignment, and of which halo particles gain or lose angular momentum can indeed be provided only in terms of resonant interactions. But one should not lose sight of the fact that such resonances lead to a large-scale density response in the halo which is the sum of the individual resonant interactions.

Weinberg and his co-workers draw attention to the delicacy of resonant interactions when the orbits of particles in fully self-consistent simulations may be diffusing because of particle noise. They argue that this problem is particularly severe for inner Lindblad resonant orbits deep in the center of the halo. Since such orbits do not accept much angular momentum, however, they contribute little to the torque on the bar and are unimportant for the principal topic of this paper. But Weinberg & Katz (2002) do claim that ensuring proper collisionless dynamics in the center is more important for halo density evolution.

The numerical experiments of Lin & Tremaine (1983) showed that a satellite orbiting a spherical system composed of much lighter particles confined in a potential well experiences a frictional force that scales very much as predicted by eq. (1), or eq. (2), despite the complications caused by resonances. This, and other evidence, led BT to conclude that “Chandrasekhar’s formula often provides a remarkably accurate description of the drag experienced by a body orbiting in a stellar system”.

We might hope that the Chandrasekhar scaling would also hold for bars, but there is no detailed check in the literature. Weinberg (1985) reports a few crude simulations of the Lin & Tremaine type in support of his theoretical calculations and he remarks (Weinberg 2004) that he has recently made more such tests. But the main point of his later paper is to highlight another complication: he shows that the LBK torque formula derived by TW84 is not the full story, and that the torque depends remarkably strongly on the past time-dependence of the perturbation.

In §4 I present a much more extensive study using the Lin & Tremaine technique for this slightly different physical problem, and show that the expected scaling of eq. (2) holds quite well. I also confirm Weinberg’s (2004) result and explore the complication of perturbation time dependence a little further. I include the effects of self-gravity between the halo particles in §5 in order to determine empirically the numbers of particles needed to reproduce the correct frictional force in fully self-consistent simulations.

### 3. HALO AND BAR MODELS

I create an  $N$ -body realization of a spherical mass distribution, which for brevity I describe as a halo, although it could be any spherical system of collisionless particles. In §4, the particles move in the smooth analytic gravitational potential of the adopted halo and I neglect any interaction forces between the particles. Since I draw the particles from a distribution function (DF) that generates the adopted halo density, the particle distribution is in equilibrium and does not evolve in the absence of an external perturbation. The isotropic halos start with no net angular momentum.

I use three quite different halo models. The first is a Hernquist (1990) model, which has the density profile

$$\rho_H(r) = \frac{M_h r_H}{2\pi r(r_H + r)^3}, \quad (3)$$

with total mass  $M_h$ . The density profile declines as  $r^{-1}$  for  $r \ll r_H$  and as  $r^{-4}$  for  $r \gg r_H$ . It should be noted that this model differs only slightly from the NFW profile (see Appendix), which appeared to be a reasonable fit to early simulations (Navarro, Frenk & White 1996) of the collapse of dark matter halos. Hernquist gives the expression for the isotropic DF that generates the halo of eq. (3). I do not employ the infinite model, but remove from the DF any particle with sufficient energy to reach  $r > 20r_H$ , so that the active mass in particles is  $\sim 0.86M_h$  while they move in the analytic potential of the untruncated halo. The active density profile is very little affected for  $r < 15r_H$ , while the bars I employ are typically much smaller, with semi-major axes  $\sim r_H$ .

I have also employed the well-known Plummer sphere

$$\rho_P(r) = \frac{3M_h}{4\pi r_P^3} \left(1 + \frac{r^2}{r_P^2}\right)^{-5/2}, \quad (4)$$

which has a uniform density core. The isotropic DF that generates this density profile is a polytrope of index  $n = 5$  (BT, equation 4-104). Again I eliminate any particle with sufficient energy to reach  $r > 20r_P$ , which is less than 1% of the mass.

As a third halo model, I have adopted the singular isothermal sphere (SIS), which formally has the scale-free density profile

$$\rho_I(r) = \frac{V_0^2}{4\pi G r^2}. \quad (5)$$

An isotropic DF that generates this density has a 1-D velocity dispersion  $\sigma = V_0/\sqrt{2}$ . The particles move in the exact logarithmic potential of the untruncated sphere, but I generate active particles from this DF with a limited range of energies. The upper bound is set so that no particle has enough energy to pass an outer radius  $r_{\max}$ , while the lower bound eliminates any particle that would be bound inside some small radius  $r_{\min}$ . I choose  $r_{\max} = 20a$  and  $r_{\min} = 0.01a$ , where  $a$  is my adopted bar semi-major axis. For this model only, I set the mass of each halo particle proportional to  $L^{1/2}$ , where  $L$  is its total angular momentum, in order to obtain a disproportionately higher density of particles in the inner parts of the halo.

The bar model is a homogeneous ellipsoid, which has

the density distribution

$$\rho_b = \begin{cases} \frac{3M_b}{4\pi abc} & \mu^2 \leq 1 \\ 0 & \mu^2 > 1 \end{cases} \quad (6)$$

where  $M_b$  is the mass of the ellipsoid,  $a$ ,  $b$  &  $c$  are its semi-axes, with  $a \geq b \geq c$ , and

$$\mu^2 = \frac{x^2}{a^2} + \frac{y^2}{b^2} + \frac{z^2}{c^2}. \quad (7)$$

I do not use the full field of this bar but employ only non-axisymmetric parts of the field, excluding the monopole term in order not to disturb the radial profile of the halo as I introduce the bar. This approach is similar to that first adopted by Hernquist & Weinberg (1992), who employed only an approximation to the quadrupole term of the bar field. Here, I determine the precise field of the bar using a multipole expansion (*e.g.* BT, §2.4), but use only the non-axisymmetric quadrupole ( $l = 2$ ,  $m = 2$ ) term, and in some cases higher terms, to accelerate the halo particles. (The odd- $l$  and odd- $m$  terms all vanish because the bar is respectively symmetric about the mid-plane and has 2-fold rotational symmetry, while the  $(l, 0)$  terms do not rotate. Because the bar lies in the equatorial plane, terms with  $l = m$  will be much larger than those with  $l > m > 0$ .) The internal and external contributions to the bar field over the radial range of the bar are tabulated only once and stored; it is straightforward to rotate the tabulated values through any desired angle at each step.

The bar rotates at angular frequency  $\Omega_b$  about its shortest axis, and I introduce the bar smoothly by increasing  $M_b$  as a cubic function of time from zero at  $t = 0$  to its final value at  $t = t_g$ . I consider the model bar to be rigid, and to spin down due to loss of angular momentum according to its moment of inertia about the shortest axis, which is

$$I = \frac{M_b}{5}(a^2 + b^2). \quad (8)$$

A rigid bar is essential for this study, even though it is unrealistic in many ways. I must make arbitrary choices for the bar mass, length, axis ratio, density profile, and initial pattern speed, rather than have all these parameters set by the dynamics of a disk. Furthermore, a bar composed of active particles will not have the same moment of inertia as a rigid figure of the same density profile, which has a pattern speed set by the mean precession rate of the bar particle orbits. Finally, the density profile of the bar should change as the bar loses angular momentum and the mean radius of the bar particles decreases, while a bar in an active disk may also grow by trapping extra orbits. The present study, however, requires rigid bars so that the bar parameters can be controlled in order to examine how friction depends on them.

The halo particles move in the combined fields of the halo and of some non-axisymmetric terms of the rotating bar field. The halo field is rigid in the experiments described in §4, but some self-gravity terms are included in §5. I sum the  $z$ -component of the net torque on the particles and use the negative of this sum as the torque acting to accelerate the bar at every step, so that the combined angular momentum of the halo and bar is conserved.

My system of units is such that  $G = M_h = r_x = 1$ , where  $r_x = r_H$  for the Hernquist halo and  $r_x = r_P$  for the Plummer halo. For the SIS models, on the other hand, I choose  $G = V_0 = a = 1$ , for which my unit of mass is  $aV_0^2/G$ . Unless otherwise stated, the bar axes are  $a : b : c = 1 : 0.5 : 0.05$  and  $t_g = 10$  in these units.

In addition to the tests reported below, I have verified that the results presented here do not depend on numerical parameters, neither are they affected when the bar field is replaced by the smooth function adopted by Hernquist & Weinberg (1992). Furthermore, Weinberg (2003, private communication) has confirmed the results reported in §5.4 with his independent code, which also agree with his perturbation theory.

#### 4. RESTRICTED SIMULATIONS

##### 4.1. Scaling with angular speed

I begin by reporting a fiducial experiment with an isotropic Hernquist halo represented by 10M particles. In this case,  $M_b = 0.01M_h$ ,  $a = r_H$ , and  $\Omega_b = 1.5$  initially. The solid curve in Figure 2(a) shows the angular acceleration of the bar, normalized by  $M_b$ , as a function of its pattern speed. Over most of the range, the drag force on the bar varies quite smoothly, peaking when  $\Omega_b \simeq 0.8$ . An initial transient, associated with the turn-on of the bar, is evident, and the curve also has a feature near  $\Omega_b \sim 0.2$ .

It should be noted that an initial pattern speed of  $\Omega_b = 1.5$  is so high that corotation lies well inside the bar, at  $r \simeq 0.274a$ . The peak deceleration of the bar occurs when corotation lies at the still unrealistically small radius  $r \simeq 0.58a$ . The pattern speed must drop to  $\Omega_b = 0.5$  to place corotation at the end of the bar, by which time the drag force is roughly one third of its peak value.

The dotted curves in Fig. 2(a) show the acceleration in a number of other experiments with lower initial starting speeds, indicating that the full friction force does not develop for some time. The convergence of the curves at lower  $\Omega_b$  shows that the prior evolution does not substantially affect the friction force in this regime. Large differences arise only at angular speeds high enough for corotation to lie inside the bar; they are discussed in §4.4.4.

Fig. 3 shows the lag angle between the principal axes of the bar and of the quadrupole response in the halo as a function of  $\Omega_b$ . I estimate the position angle of the halo density response from the phase of the (2,2) component of a high radial order spherical Bessel function (*e.g.* Arfken 1985) transform of the particle distribution. It is clear that the response lags the bar by almost a right-angle at high  $\Omega_b$ , and the lag angle decreases continuously as the bar slows, becoming nearly aligned with the bar when its rotation speed is very low. Comparison with Fig. 2(a) confirms, as it must, that the torque is weak when the response is almost orthogonal to, or aligned with, the bar and is greatest as the phase lag passes through intermediate angles. (Since the magnitude of the torque also depends on the amplitude of the response, the maximum need not be when the response is precisely  $45^\circ$  out of phase, although it clearly occurs close to this angle.)

Fig. 2(b) shows the much stronger frictional deceleration for a thinner bar with axis ratios 1:0.2:0.05. The quadrupole potential of this bar peaks at about twice the value of the fatter bar used in Fig. 2(a), but at a smaller

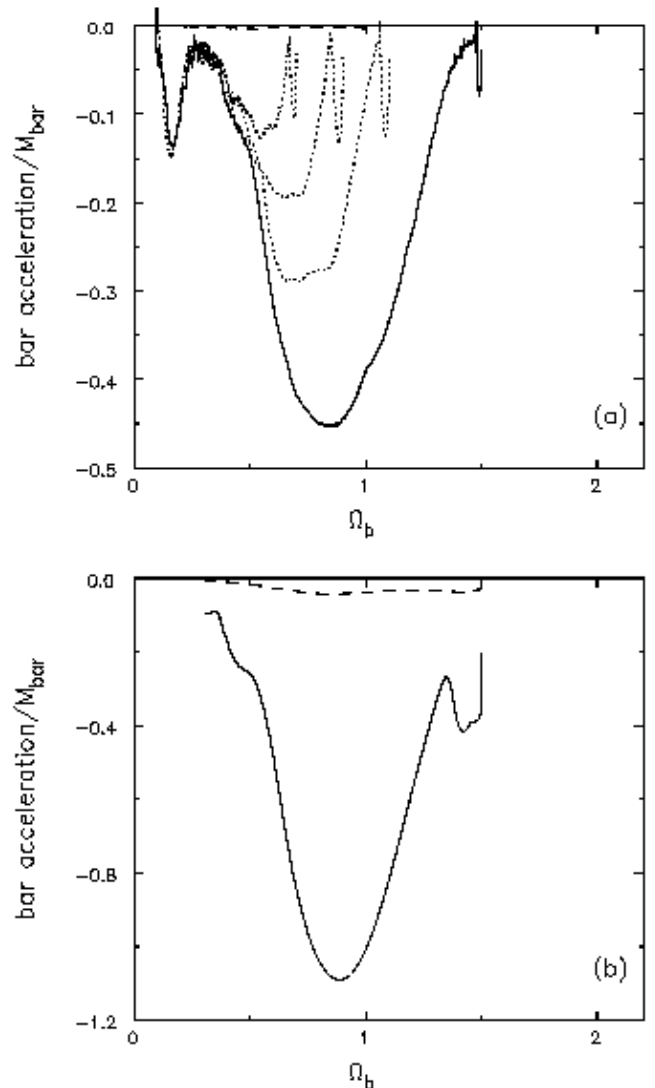


FIG. 2.— The angular acceleration of the bar, normalized by  $M_b$  as a function of angular speed. (a) The solid curve shows the acceleration in response to the quadrupole field of the bar for  $M_b = 0.01M_h$  in the fiducial run; the dotted curves are for different initial  $\Omega_b$  values. The dashed curve shows the same quantity when the perturbing force is the (4,4) component of the bar field only for  $M_b = 0.2M_h$ . (b) As for (a), for a thinner bar with axis ratios 1:0.2:0.05. Note the different scales between the two panels.

radius; the two fields could not be matched by scaling, therefore. Nevertheless, the curve has a similar shape.

The dashed curves in both panels of Fig. 2 show the frictional deceleration for a 20 times more massive bar when only the  $l = 4$ ,  $m = 4$  term of the bar field is used to force the halo. Since the evolution with a 1% mass bar is impracticably slow, I used a 20% mass bar in both cases, and normalized all curves in this Figure by the separate bar masses. The relative strengths of the quadrupole and higher-order components of the perturbing field depend on the bar shape; the (4,4) component of the potential has a peak amplitude of  $\sim 1/6$  that of the quadrupole for the

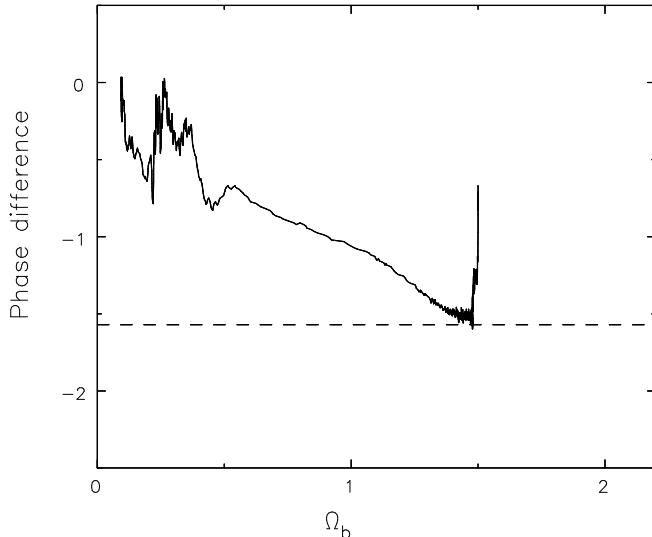


FIG. 3.— The phase lag in radians between the density response in the inner halo and the bar from the fiducial run shown in Fig. 2(a). The response is approximately orthogonal to the bar direction when  $\Omega_b$  is large, and gradually shifts into alignment as the bar slows.

fatter bar, whereas it is a larger fraction ( $\sim 1/3$ ) for the thinner bar. Yet the contribution to friction from the (4,4) term is small even for the sharper bar (Fig. 2b); higher order terms will be still less important.

Since friction is dominated by only the lowest-order, non-axisymmetric term of the potential, it is possible for even low-spatial resolution codes, such as that used by Debattista & Sellwood (1998, 2000), to reproduce the frictional drag quite accurately. Thus the suggestion by Valenzuela & Klypin (2003) that their different result was due to inadequate spatial resolution in the earlier work is unlikely to be correct. The different results obtained in these two studies will be discussed further in Paper II.

#### 4.2. Interpretation

The phase angle of the halo response shown in Fig. 3 is not hard to understand. The following argument is specific to spherical potentials, but it generalizes to aspherical cases.

Orbits in a spherical potential have only two frequencies because they move in a single plane. The angular frequency of their mean motion about the center is, in general, incommensurable with the angular frequency of their in-and-out radial motion. However, there is a set of rotating frames, with frequencies  $\Omega_{km}$ , from which an observer would see the orbit close after  $k$  turns and  $m$  radial oscillations (*e.g.* Kalnajs 1977). Resonant orbits are those which close in the frame of the perturbation, which rotates at frequency  $\Omega_b$ . Note that in a spherical potential  $|\Omega_{km}|$  is the same no matter what the angle between the orbit plane of the particle and the rotation axis of the bar, but the sign of  $\Omega_{km}$  will differ for direct and retrograde particles.

Most orbits are not resonant, however, and  $\Omega_{km} \neq \Omega_b$  for any  $(k, m)$ . For these general orbits, the perturbation

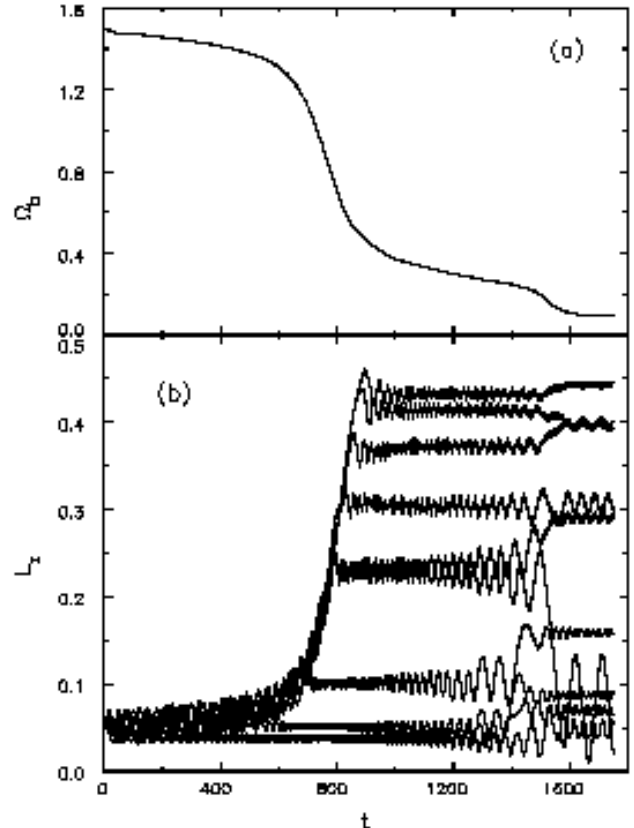


FIG. 4.— (a) The evolution of the pattern speed in the fiducial run. (b) The instantaneous angular momenta of ten particles as a function of time. The particles move in the mid-plane and all start with the same energy and angular momentum but have equally spaced phases. The quasi-periodic oscillations on each line are the forced response to the bar potential, the large changes, which are not modulated for the most part, are caused by passages through resonances.

adds to its otherwise axisymmetric time-averaged density, a forced non-axisymmetric distortion that corotates with the bar. As happens for simple harmonic oscillators, the driven response is in phase, or aligned, with the bar when  $\Omega_b < \Omega_{km}$ , and is perpendicular to the bar for higher bar pattern speeds. Thus the forced response of an orbit switches from perpendicular to alignment as the bar slows across its resonant frequency; the change of phase is gradual because the resonance is broadened by the changing pattern speed. Since many orbits are present with a wide range of precession rates for each resonance, the net response is the aggregate of many orbits.

Angular momentum can be exchanged between the particles and the bar when the resonance sweeps through. The time evolution of the pattern speed of the bar in the fiducial experiment is shown in Fig. 4(a), while Figure 4(b) shows the evolution of the instantaneous  $L_z$  for ten particles orbiting in the mid-plane. The orbits shown are those of test particles run in a reconstruction of the time evolution of the total potential, which requires knowledge only of the bar phase at every step in the original simulation.

All have the initial energy  $E = 0.7$  and angular momentum,  $L_z = 0.5L_{\max}(E)$  but are spaced equally in initial phases. The short-period oscillations in  $L_z$  of each particle are forced as each particle moves in the bar field. Larger, and lasting, changes occur as particles pass through a resonance. Individual orbits can either gain or lose, depending on their phase relative to the bar, but generally an excess of gainers leads to the observed friction.

The particular group of particles selected undergo unusually large changes, much greater than average. The largest occur over the time interval  $t = 600$  to  $t = 800$  during which time  $\Omega_b$  decreases most rapidly, from  $\sim 1.4$  to  $\sim 0.6$ . Six out of the ten particles gain in angular momentum by a factor  $\gtrsim 5$  as they are caught in a corotation resonance, while the particles whose orbital phases are unfavorable for a strong interaction at this resonance suffer much smaller changes. Some particles also pass through an inner Lindblad resonance between  $t = 1400$  and  $t = 1600$ ; one such particle gives up most of the angular momentum it had gained earlier. Notice that friction is strongest when these particles pass through corotation, and that the late second blip in friction (Fig. 2a) occurs as the particles pass through the inner Lindblad resonance. The particles shown were deliberately selected to illustrate this feature.

TW84 note that the frictional torque will be reduced, and the sign of the exchange between the particle and the perturbation difficult to predict, if the halo particles pass slowly through the resonance (as defined in §2). TW84 and Weinberg (1985) expected fast passage through the resonance, but offered no proof. Diagrams such as Figure 4(b) allow us to examine this key issue. The largest changes for each particle are generally non-oscillatory, indicating that the particle is not librating in the resonance, and therefore the passage is fast.

Quite different behavior can be seen for some late changes to the particles having most angular momentum. They also undergo modest long-term changes in  $L_z$ , which instead take place over many forced oscillations. In these cases the short-period oscillations are adiabatically invariant, and the change in the mean  $L_z$  again seems to be mostly monotonic.

Thus Figure 4(b), and hundreds of other orbits that I have examined, show that most passages through resonance can indeed be treated by the LBK approach. Since I have not examined every corner of phase space, this does not, of course, amount to a proof that the LBK formula holds for all orbits, but it does suggest it is good for most orbits.

The dashed curves in Fig. 2 show that the (4,4) component of the perturbing potential makes only a modest contribution to the total friction force, even for the thin bar where it has a significant amplitude. As for the dominant quadrupole term, angular momentum exchange should take place at resonances, but such resonances are of higher-order, which have weaker effective potentials and therefore influence smaller fractions of phase space than do the lower-order resonances. Thus these resonances are of lesser dynamical importance, causing higher-order components of the potential to add disproportionately little to the friction force.

#### 4.3. Other halo density profiles

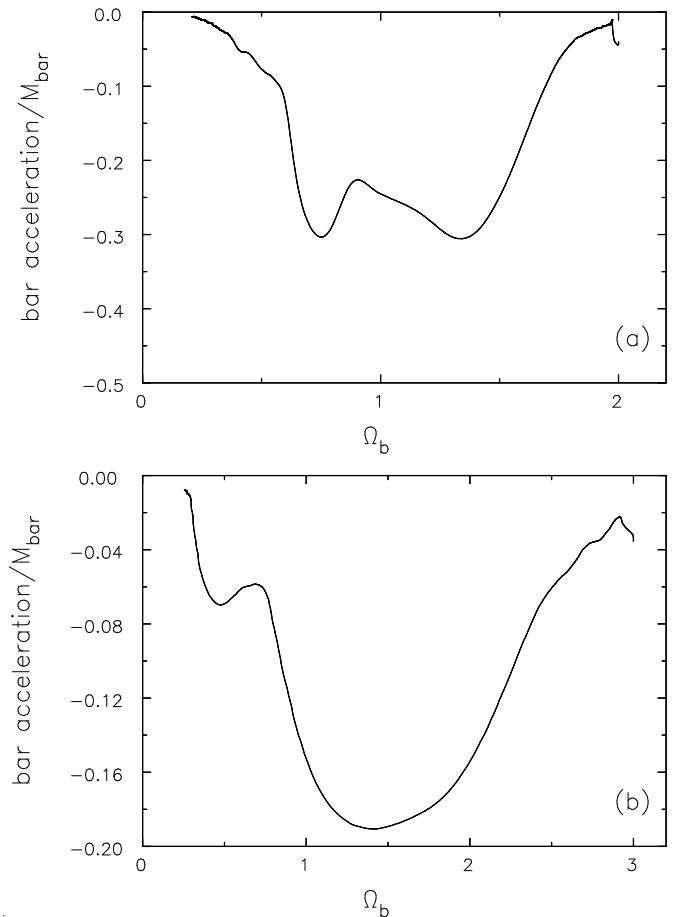


FIG. 5.— As for Fig. 2(a), but (a) for the Plummer halo and (b) for the singular isothermal sphere.

Figure 5(a) shows the acceleration as a function of angular speed for the Plummer halo, while Fig. 5(b) is for the singular isothermal sphere (SIS). These are directly comparable with Fig. 2(a), which is for the Hernquist halo. The angular velocity dependence of the frictional acceleration is noticeably different in both cases.

The bar in the Plummer halo has a semi-major axis  $a = R_P$  and a mass  $M_b = 0.02M_h$ . Friction has two approximately equal peaks when  $\Omega_b \simeq 1.4$  and  $\Omega_b \simeq 0.7$ , but the angular speed of this bar must drop to  $2^{-3/4} \simeq 0.6$  before corotation moves outside the bar.

The behavior for the SIS is different again. Corotation is at the end of the bar when  $\Omega_b = 1$ , where friction is again past its peak. Note that features can arise in this curve because the scale-free nature of this model is broken in two ways: the perturbation has a definite linear size and the energy range of the active particles is restricted. The mass of the bar in this case,  $M_b = 0.2aV_0^2/G$ .

These curves, and that in Fig. 2(a), indicate the functional form of  $\Theta$  in eq. (2). Since the bar is the same in all three cases, the differences stem directly from differences in the halo mass profiles, which affect the frequencies and particle density at the different resonances. Such differences are the analog of having a different velocity distribution for the background particles in the Chandrasekhar problem.

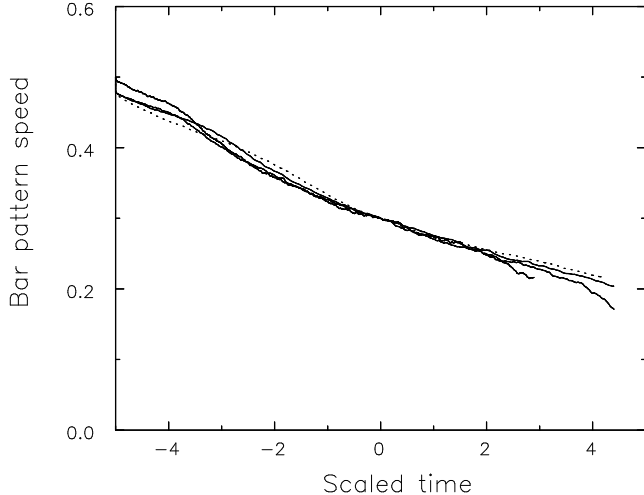


FIG. 6.— The bar pattern speed as a function of normalized time for a series of experiments with differing mass bars, but all other properties held fixed. Bar masses are 0.5%, 1%, & 2% (all solid lines) and 5% (dotted line) of the halo mass. The times are scaled by the bar masses and shifted horizontally to coincide when  $\Omega_b = 0.3$ .

#### 4.4. Scaling with other parameters

In this section, I check directly whether the acceleration scales with bar mass, halo density and halo velocity dispersion, as suggested by eq. (2). All experiments reported in this section employ 10M particles, as were also used for those shown in Figs. 2 & 5. I illustrate these tests for the Hernquist halo; the other halo models scale about as well, except for the test with velocity dispersion, as discussed in §4.4.3.

##### 4.4.1. Scaling with bar mass

Figure 6 shows the time evolution of the pattern speed for bars of different masses, in the Hernquist halo; the bar pattern speed is a smoother function than its acceleration. Each line in this figure is from a run with a different bar mass in the range  $0.005 \leq M_b/M_h \leq 0.05$  and  $\Omega_b = 0.5$  initially; the time axis is scaled by  $M_b$ , and the curves have all been shifted horizontally to coincide at the moment at which  $\Omega_b = 0.3$ . The curves overlay almost perfectly, indicating that frictional acceleration scales linearly with  $M_b$  in this regime, as expected from eq. (2).

Note that the argument that resonant passages are fast is not altered by changes to the mass of the bar. Even though  $|\dot{\Omega}_b|$  increases directly as the bar mass, the disturbance potential, which essentially sets the range of particle frequencies affected by the resonance, is narrower by the same factor. Therefore, the applicability of the LBK approach is largely unaffected by the mass of the bar; TW84 estimate that slow transitions for the satellite decay problem make an order unity change to the LBK torque only for satellite masses  $\lesssim 10^{-6}$  of the interior halo mass.

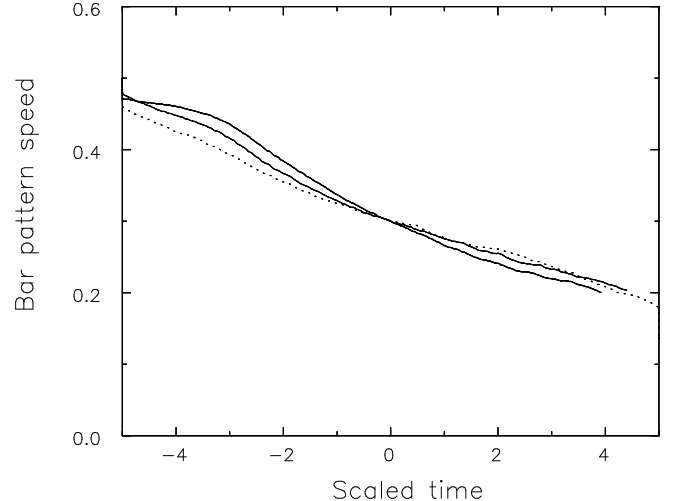


FIG. 7.— As for Fig. 6, but for the case when the halo density is scaled. The dotted curve is for the case when the halo density is doubled. See §4.4.2 for details.

##### 4.4.2. Scaling with halo density

Equation (1) predicts that the acceleration is proportional to the density of the background. In the present more realistic case, the density of the background varies with radius and it might seem that I would have to evaluate the LBK torque for a number of different halos to obtain a testable prediction. Fortunately, there is a much simpler way to test for the density dependence: I simply scale the density of the entire halo without changing the potential well in which the particles move. This ploy is equivalent to treating some fraction of the halo as rigid if the density is reduced but, since the density and potential of the halo need not be self-consistent in these restricted experiments, it is also possible to increase its density. I adopt this admittedly artificial strategy here simply to test for the expected linear scaling.

Figure 7 shows the results with a 2% mass bar, with Hernquist halos that have 0.5, 1 and 2 times the density given in eq. (3). Again the time axis scale is proportional to the density, and curves are shifted so that they coincide when  $\Omega_b = 0.3$ . While not quite as convincing as Fig. 6, the similarity of the curves shows that the expected linear scaling holds approximately, in satisfactory agreement with the prediction of eq. (2).

##### 4.4.3. Scaling with halo velocity dispersion

Finally, I test the scaling with velocity dispersion predicted by eq. (2). Again I employ a trick: by scaling the gravitational potential by a factor, and the velocity dispersion,  $\sigma$ , by the square root of the same factor, we continue to have an equilibrium model with an unchanged density profile. (The halo density and potential are no longer self-consistent, of course.) For this series of tests, however, I must also scale the bar pattern speed, since the argument of  $\Theta$  contains the dispersion,  $\sigma$ .

Figure 8(a), which plots  $\Omega_p/\sigma$  as a function of  $t\sigma^{-3}$ , shows that when the velocity dispersion is increased or decreased by a factor  $\sqrt{2}$ , the evolution of the scaled bar angular speed does vary at approximately half or double the

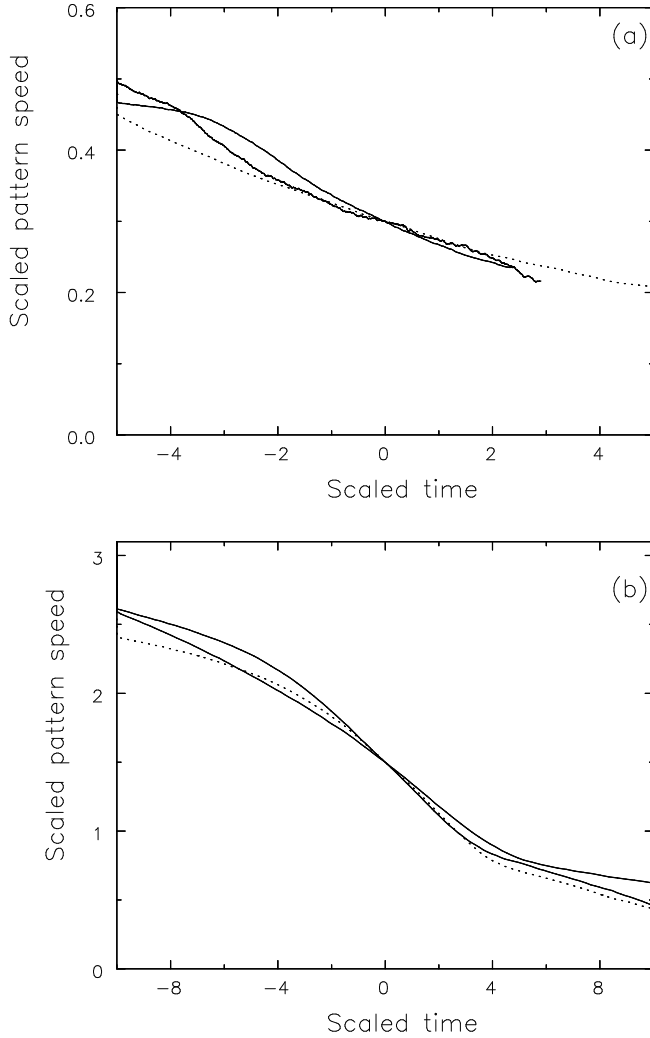


FIG. 8.— (a) As for Fig. 6, but for the case when the halo velocity dispersion and potential are scaled. The dotted curve is for the largest velocity dispersion. (b) Same as (a), but for the singular isothermal sphere. See §4.4.3 for details.

rate, respectively, as predicted by eq. (2), but the curves do not match up as well as in Figs. 6 & 7.

Since scaling the potential well affects all the resonances, the particle density at each resonance does not scale in a simple manner, and formula (2) is too naïve. However, scaling should be restored in a scale-free model. The same scaling test with the SIS supports this expectation; the curves in Fig. 8(b) follow each other more closely than in Fig. 8(a), which was for the Hernquist halo.

#### 4.4.4. Bar turn-on

Weinberg (2004) compares results from experiments similar to those reported here with his analytic formulae. The solid curve in Figure 9 shows the pattern speed evolution using my code with the bar and NFW halo that Weinberg employed for his first test. The axes have been scaled to the units adopted by Weinberg (see Appendix). The time evolution of the pattern speed is in excellent agreement with his time-dependent, linear theory predic-

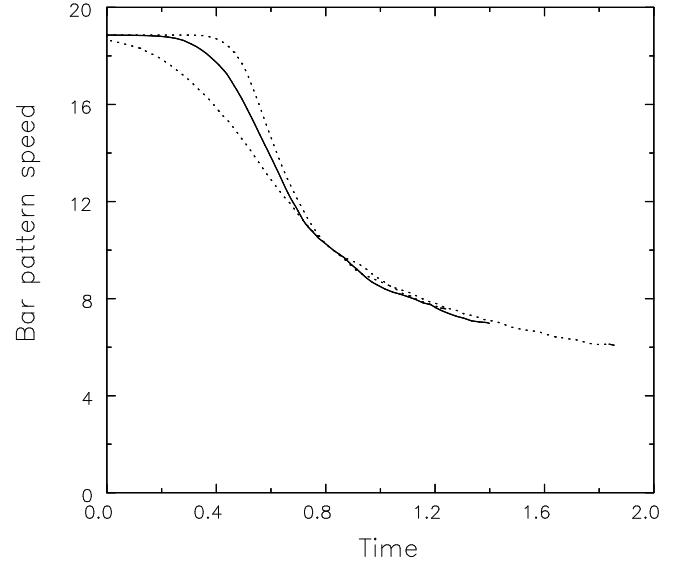


FIG. 9.— Confirmation of Weinberg's (2004) result (solid line) and two other similar models (dotted lines) with more abrupt and slower bar turn-on. See §4.4.4 for details.

tion, as is the simulation he presents. Thus there is little room to question the performance either his or my  $N$ -body codes in this idealized situation.

However, Weinberg's main finding is that the LBK torque formula from TW84 does not predict the correct time evolution of the bar pattern speed; he was able to obtain close agreement with the experimental results only by taking the growth of the bar perturbation into account. His formula for the torque in the time-dependent regime is also of the form eq. (2), but with a function  $\Theta$  that now depends on the entire history of the perturbation.

The dotted curves in Fig. 9 (which have been shifted horizontally to coincide with the solid curve when  $\Omega_b = 10$ ) show that the dependence on the turn-on rate affects the initial friction force, but not the later evolution. The dotted curves in Fig. 2(a), on the other hand, indicate a much stronger, and long-lasting, dependence on the initial pattern speed. It is important to note that the curves converge when  $\Omega_b$  has dropped to a realistic value. Furthermore, the eventual convergence of these curves suggests that the differences are not due to changes in the DF caused by the earlier evolution. It seems likely that the time-dependence discovered by Weinberg is the main reason that these curves take so long to converge.

Figs. 6 – 8 show that the scaling of the frictional force with the main parameters of eq. (2) still holds, at least approximately, despite the complication of time-dependence, as Weinberg also notes. Note that the perturbation has the same initial  $\Omega_b$  and turn-on rule for the bar mass and halo density tests, so that the time-dependence of the function  $\Theta$  did not change. However, the initial bar pattern speed had to be scaled in the experiments with different velocity dispersion, making the reasonable agreement shown in Fig. 8(b) all the more reassuring.



#### 4.4.5. Summary

The present problem differs from that considered by Chandrasekhar in many ways: the perturber is an extensive rigid body moving at changing angular frequency through an inhomogeneous sea of particles, which encounter the perturbation in a periodic fashion. Yet, this series of experiments has demonstrated that the deceleration of the bar caused by dynamical friction from non-interacting halo particles scales with bar mass and halo density as predicted by eq. (2), which so closely resembles Chandrasekhar's formula (1). The naïve scaling with velocity dispersion holds approximately for a general halo, and rather better for a self-similar halo, such as the SIS. The scaling with these parameters is an inevitable consequence of dynamical friction being second order effect caused by the interaction between the perturber and its own wake.

The importance of time-dependence is disconcerting, however, since friction depends slightly on how the bar was turned on (Fig. 9), and strongly on the choice of initial pattern speed (Fig. 2a)! The arbitrariness of these parameters makes experiments with imposed bars all the more artificial.

#### 4.5. Convergence test

As noted earlier, halo particles gain angular momentum, on average, at resonances. Even though each may pass through the resonance rapidly, we will not obtain the smooth torque expected in the continuum limit unless there are many particles, densely spread over a broad range of resonant frequencies. The required number depends on the width of the resonance in frequency space: If the bar had a fixed or very slowly changing pattern speed, the resonances would be sharp and the simulations would indeed require a very large  $N$  (Weinberg & Katz 2002; Holley-Bockelmann, *et al.* 2003), but the forcing frequency is broadened by its decreasing angular speed and we can hope that the discreteness of the particle distribution will become insignificant for some attainable  $N$ .

Figure 10 shows that the pattern speed evolution in the Hernquist halo appears to converge to a smooth function as  $N$  increases. Merely  $10^4$  particles are sufficient to obtain qualitatively correct behavior for the 5% mass bar, but perhaps one hundred times larger  $N$  is needed for comparable numerical quality with a bar of one tenth this mass. Phase space needs to be populated more densely as the mass of the bar decreases, in order that a large enough number of particles are passing through the resonance at any time to yield a smoothly varying force. Both the effective potential of the resonance is weaker, and the Lorentzian frequency width of the resonance is reduced by the slower braking rate. As both factors scale linearly with the mass of the perturber, it seems reasonable that the number of particles needed to obtain smoothly varying friction should vary as  $M_b^{-2}$ .

The smoothness of the braking rate in Figs. 2 & 5, and for large  $N$  in Fig. 10, is evidence that the resonant exchanges which give rise to the force are dense enough at most frequencies to produce a smooth torque. The frictional force may become erratic because phase space is not populated densely enough at very low pattern speed as  $|\Omega_b|$  decreases, but this is a physically uninteresting

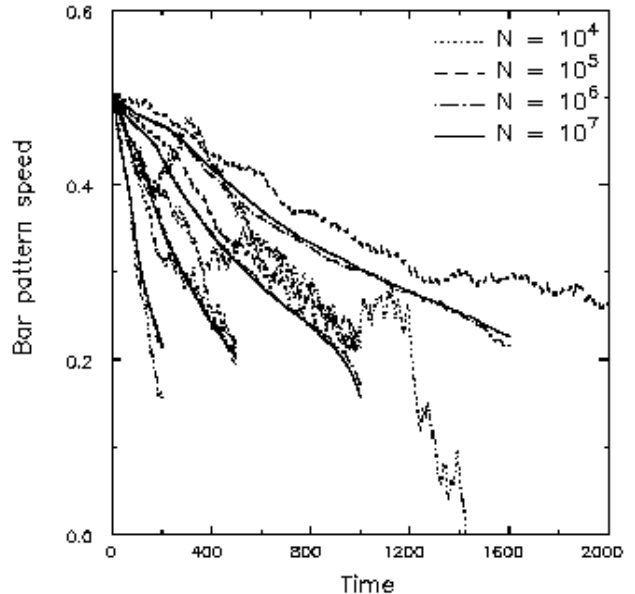


FIG. 10.— The bar pattern speed as a function of time for experiments with differing mass bars, each for four separate values of  $N$ . The line styles indicate the number of particles, with the solid line being for the largest  $N$ . The four groups of lines are for  $M_b/M_h = 0.005, 0.01, 0.02$ , &  $0.05$  and the decay rate increases with bar mass.

regime.

It should be noted that these experiments reveal only the number of particles needed to populate phase space densely enough for the frictional force to approximate the continuum limit in the absence of self-gravity. The issue of collisional relaxation also needs to be addressed when the particles interact with each other, which may require more particles, as I discuss in §5.3.

#### 5. EFFECT OF SELF-GRAVITY IN THE HALO

The experiments just reported treat the halo as a non-interacting population of test particles, which move in a fixed potential well and respond only to the perturber, as in the usual treatment of dynamical friction (*e.g.* BT). Collective effects in a collisionless halo could also be important, however, because the wake itself contributes to the non-axisymmetric density affecting the orbits of the halo particles. Hernquist & Weinberg (1992), Weinberg & Katz (2002), and Sellwood (2003) have already reported some experiments with rigid bars that take this into account, but the emphasis in those papers was on the change to the halo density profile.

Here I study the effect of self-gravity on the frictional force, while still employing an imposed bar. I break the discussion of collective effects into two levels of complication: when self-gravity includes the monopole terms, the radial mass profile of the halo could possibly change substantially over time, as claimed by Weinberg & Katz (2002). I therefore begin by including only the quadrupole field of the response density, before describing how other terms affect the evolution. Note that all the experi-

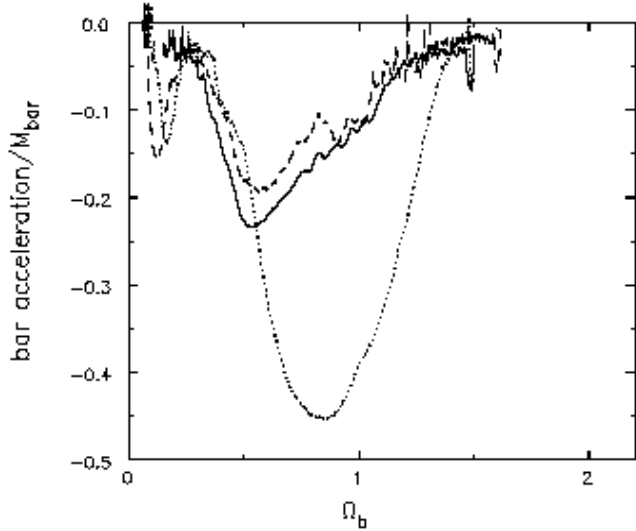


FIG. 11.— The acceleration of the bar when self-gravity of the halo response is included. The solid curve shows the behavior when all terms  $0 \leq l \leq 4$  are included, the dashed curve shows the situation when only the  $l = 2$  terms are employed. The dotted curve shows the corresponding case with no self-gravity, the fiducial model, reproduced from Fig. 2(a).

ments described in this paper are perturbed with the non-axisymmetric field of a rigid bar. Fully self-consistent simulations, with the bar also made of responsive particles, are reported in other work (*e.g.* Paper II).

I compute the self-gravity of the halo using the PM+SH method described in Appendix A of Sellwood (2003). Briefly I use a 1-D spherical grid, with an expansion of the gravitational field up to order  $l_{\max}$  in surface harmonics on each radial shell of the spherical grid.

### 5.1. Quadrupole field of the response

The dashed curve in Figure 11 shows the bar acceleration when only the quadrupole field of the halo response density is included; the dotted curve, reproduced from Fig. 2(a), shows the behavior with no self-gravity. It is clear that the self-gravity term increases the drag slightly when the pattern speed is low, but greatly *diminishes* it when the bar has an artificially high pattern speed.

This behavior is a consequence of the phase of the halo response. Including the self-gravity of the response weakens the net torque on the bar when the response is more than  $45^\circ$  out of phase with the imposed bar; the phase lag when self-gravity is included is somewhat similar to that shown in Fig. 3, but the response remains more nearly perpendicular for longer. As the bar slows, the response gradually shifts towards alignment with the bar, thereby augmenting the quadrupole field of the perturbation and causing modestly increased friction. Note that friction peaks at  $\Omega_b \simeq 0.5$  when corotation is at the end of the bar, implying that self-gravity always enhances friction in the physically relevant regime.

### 5.2. Including the monopole and other terms

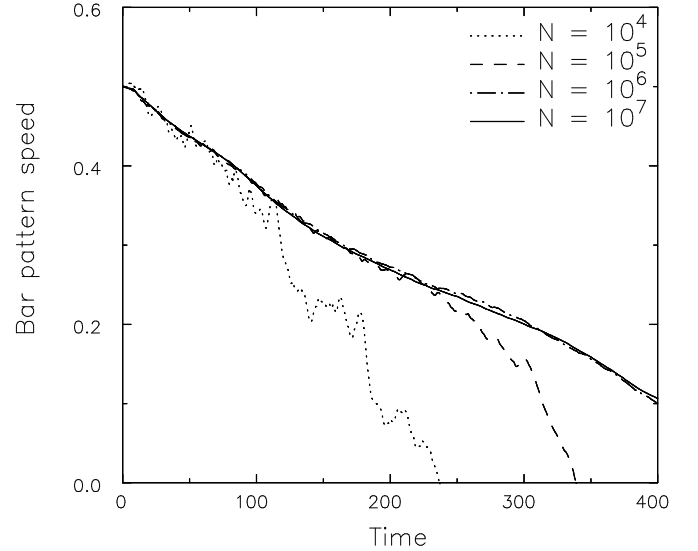


FIG. 12.— The evolution of the pattern speed of a 2% mass bar which starts with corotation at the end of the bar ( $a = r_H$ ), for experiments with different  $N$ . Unlike for Fig. 10, these experiments include all low-order self-gravity terms of the halo particles ( $l \leq 4$ ).

The solid line in Fig. 11 shows the effect of adding more terms to the self-gravity of the halo response; in this case all  $l \leq 4$  terms. Additional self-gravity terms increase friction somewhat over that obtained with  $l = 2$  only at most angular speeds.

### 5.3. Convergence test

Figure 12 shows the effect of changing the particle number  $N$  in a somewhat realistic case in which the imposed bar starts at an angular speed such that it just fills its corotation circle. This test includes all  $l \leq 4$  terms of the self-gravity of the halo density response, and thus some collisional relaxation must be present. These experiments are with the Hernquist halo and a bar with  $M_b = 0.02M_h$ .

As without self-gravity, the time variation of the pattern speed becomes smoother as  $N$  increases. The evolution is closely similar for the two cases with  $N \geq 10^6$ , but friction is clearly overestimated when  $N = 10^4$  and slightly so when  $N = 10^5$ . The minimal differences between the results for the experiments with  $N = 10^6$  and  $N = 10^7$  indicate that 1M particles is a sufficient number to capture the correct physics for this case with a low-mass bar.

The 2% mass bar used in Fig. 12 is the same as for the second most strongly braked case in Fig. 10. Comparison of these two convergence tests indicates that the low- $N$  models depart more strongly from the high- $N$  results when self-gravity is included. However, the number of particles needed for convergence is not increased dramatically by self-gravity.

Thus, Weinberg & Katz (2002) and Holley-Bockelmann, *et al.* (2003) are correct that the reduction in orbit quality caused by numerical noise in self-gravitating halos does affect the friction force, but the torque converges for reasonably accessible numbers of particles; 1M appears to be plenty in this problem, as Sellwood (2003) concluded from fully self-consistent experiments.

Holley-Bockelmann, *et al.* (2003) report fully self-consistent experiments for which the behavior with  $N = 1\text{M}$  differs from similar experiments with larger  $N$ . However, the difference does not necessarily support their conclusion that  $1\text{M}$  particles is inadequate for bar-halo interaction. They show (their Fig. 20) that the quadrupole field in the  $1\text{M}$  particle experiment is weaker, so the halo torque *must* also be weaker, which implies that the lower halo particle number could still be adequate. Both Weinberg & Katz (2002) and Sellwood (2003) report that smaller  $N$  leads to more rapid angular momentum transfer, as also shown in Fig. 12, making the inadequate- $N$  interpretation in this case still less plausible. Holley-Bockelmann, *et al.* do indeed have a result that is  $N$ -dependent, but the effect of lower particle number is to decrease the strength of the  $m = 2$  distortion in the disk, and is therefore a consequence of disk dynamics and not halo friction. It is likely that a higher noise level in their lower- $N$  disk interferes with their bar triggering mechanism. Specifically, they start with a bar-unstable disk and also apply a transient tidal field to trigger the bar; the smaller the number of particles, the larger the initial amplitude of the intrinsic instability, which will generally interfere with the applied tidal field leading to a weaker bar, unless the phases of the two bar-forming mechanisms happened to be nearly aligned.

#### 5.4. Halo density changes

Hernquist & Weinberg (1992) found that the inner density of the halo may be reduced substantially by interactions with a bar in experiments that have been subsequently confirmed and elaborated by Weinberg & Katz (2002) and by Sellwood (2003). Little evolution is expected without self-gravity (Sellwood 2003), but the profile is hardly altered even in the above self-consistent experiments with mostly rather light bars.

Bars with stronger quadrupole fields do indeed reduce the halo density, as shown in Figure 13(a). The changes to the initial Hernquist mass profile are brought about by friction with a bar with  $M_b = 0.1M_h$ , axes  $a : b : c = 1 : 0.2 : 0.05$ ,  $a = r_H$ , and initially  $\Omega_b = 0.5$  so that the bar fills its corotation circle. Once again, the bar is represented by its quadrupole field, and the evolution of this  $N = 1\text{M}$  particle model includes the  $l = 0, 2$  &  $4$  terms of the response self-gravity. However, a bar of half the mass and length, and an appropriately higher initial angular speed, produces very little change, as shown in Figure 13(b). Because of the concerns raised by Weinberg & Katz (2002), I increased the number of halo particles in this experiment to  $N = 10\text{M}$ . The bar pattern speed had dropped by a factor of  $\sim 4$  by the end of this simulation, when the frictional drag is well past its peak. These results have been confirmed by Weinberg (2003, private communication) in independent tests with his code and using his perturbation theory.

Inclusion of odd- $l$  terms with more massive, rigid, imposed bars often causes the halo to become lop-sided. The resulting unphysical forces transfer angular momentum at a greatly enhanced rate and cause large density changes relative to the fixed center about which the bar rotates. The proper way to deal with such an artifact is to treat the entire system self-consistently, when it is found that inclusion of odd- $l$  terms makes little difference to the torque

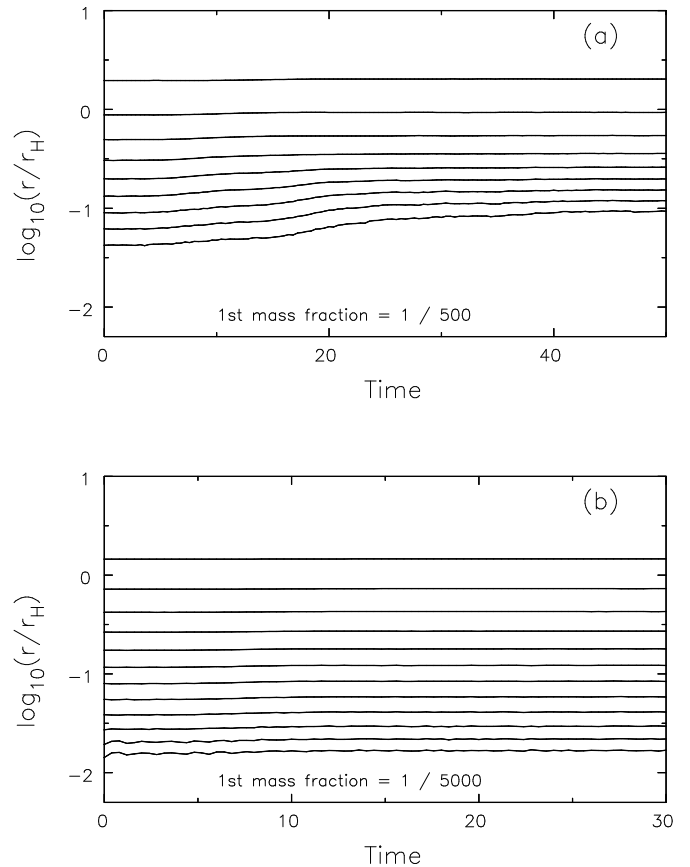


FIG. 13.— The evolution of radii of fixed mass fractions of the halo. Successive curves are for fractions that increase by factors of two, starting from the smallest given fraction. The mass of the bar is 10% of that of the Hernquist halo in (a), while it is 5% in (b).

(Sellwood 2003; Holley-Bockelmann, *et al.* 2003).

It is expected that a bar in an NFW halo would have a mass of a few percent of the halo mass, and a semi-major axis about one quarter of the distance to the radius of the knee in the density profile. Realistic bars are clearly not going to cause substantial changes to the density profile, as reported by Sellwood (2003).

## 6. CONCLUSIONS

I have shown that dynamical friction between a rotating, imposed bar and a halo scales in a very similar manner to that predicted by Chandrasekhar's formula. The experiments reported in §4 are highly idealized and employed the simplest possible system that could capture dynamical friction on a bar rotating in a halo. The retarding acceleration depends on the angular speed of the bar, scales linearly with its mass (*i.e.* the strength of its quadrupole field) and with the background density. It also scales roughly inversely as the square of the velocity dispersion of the background through which it moves, although this scaling is more approximate unless the model is self-similar. This result is the analog for a bar of that obtained by Lin & Tremaine (1983) from a similar study with orbiting satellites.

Even though the physical situation is quite different from rectilinear motion through an infinite, uniform background, and complicated by the existence of resonances and bar turn-on issues, the Chandrasekhar scaling still holds. It holds, because dynamical friction is fundamentally a second order effect that arises from the interaction of a perturber with its own wake. The strength of the interaction does depend on the details, but the parameter scaling cannot.

Tremaine & Weinberg (1984) first demonstrated that friction arises as the perturbation sweeps across resonances with the particles, a point stressed in recent work by Weinberg and his co-workers and by Athanassoula (2003). I have shown that the pattern speed of the bar changes sufficiently rapidly that a halo particle generally passes through the resonance without any complicated non-linear trapping, as expected by TW84. The forced responses of the halo particles change from anti-alignment to alignment with the bar as the pattern speed crosses a resonance, which happens smoothly because the resonance is broadened by the changing pattern speed. The net effect is to produce a global density response that lags the bar, causing the frictional drag.

In all three halo types employed here, friction is weak when the bar pattern speed is so high that corotation is well inside the bar. As the bar slows, the frictional drag grows at first but generally peaks before corotation reaches the bar end. Thus, in the physically interesting regime, where corotation is beyond the end of the bar, friction always decreases as the bar slows in these non-rotating halos. A preliminary study of the effect of rotation in the halo was reported by Debattista & Sellwood (2000), who found that friction is weaker when the halo rotates in the same direction as the bar, and stronger when the halo counter-rotates, in comparison with a non-rotating halo. Since lowest order effect of halo rotation is to change the relative speed of the bar through the background, these earlier results are consistent with the finding here (*e.g.* Fig. 2) that friction increases as the bar rotates faster whenever corotation is outside the bar.

Friction is dominated by the quadrupole field of the bar both because the quadrupole is the dominant potential component of the bar, but also because the higher-order resonances that are associated with the higher expansion terms couple less strongly to the particles. Since the lowest-order, non-axisymmetric component of the bar field dominates, friction can be captured adequately in simulations with even quite low spatial resolution, provided enough particles are employed.

In the absence of self-gravity, the number of particles needed to obtain a smoothly varying frictional force is quite modest, unless the bar is very weak. The main requirement here is that the broadened resonances caused by the time-varying pattern speed should overlap many particles in order to obtain the correct density response. The pattern speed changes more slowly for weaker bars, making the resonances narrower and consequently raising the particle number needed to obtain a smoothly varying force. The number of particles needed in this regime rises as the inverse square of the quadrupole field strength.

Weinberg & Katz (2002) argue that collisional relaxation in simulations with self-gravity should increase the

number of particles required to approach the continuum limit, because potential fluctuations arising from Poisson noise affect the orbital behavior. The lowest-energy orbits, which they find are most delicate, should make a negligible contribution to the torque. I have found a small reduction in force quality when self-gravity is included, consistent with the prediction by these authors, but quite modest particle numbers are needed to bring this problem under control. Thus the frictional torque can be simulated accurately with standard algorithms and readily accessible computers.

The halo density profiles were hardly altered in all experiments reported here, except for the case shown in Fig. 13(a), which employed a huge, massive bar. Weinberg and his co-workers (in preparation) argue that delicate resonant effects deep in the cusp can lead to density reductions, which are easily suppressed by numerical noise in all but the most careful simulations. The process they discuss does not, however, affect the ability of more modest simulations to reproduce the correct frictional drag.

All experiments reported here employ an imposed bar potential in order to examine the dependence of the halo response on the bar parameters. This simplifying approximation has many obvious disadvantages, as noted in §3. Weinberg (2004) uncovered a further unforeseen complication – that the friction force depends not only on the bar’s instantaneous amplitude and pattern speed, but also the past history of these quantities! I have confirmed and slightly elaborated his troublesome finding. It is clear that artifacts of this type make imposed bars still less realistic. Fully self-consistent simulations, such as those to be reported in Paper II, are the only way to ensure that the bar forms with a dynamically realistic amplitude and pattern speed and responds to friction in the appropriate way.

I am grateful to Martin Weinberg for very helpful discussions, running some tests for comparison, sending a draft of his preprint, and for detailed comments on this manuscript. I also thank Victor Debattista for his input and Scott Tremaine for comments on an early draft of this paper. This work was begun while the author was a visiting member of the Institute for Advanced Study in Princeton; their hospitality is gratefully acknowledged. Grants from NASA (NAG 5-10110) and from NSF (AST-0098282) provided support.

## REFERENCES

- Arfken, G. 1985, *Mathematical Methods for Physicists*, 3rd ed. (Orlando: Academic Press)
- Athanassoula, E. 1996, in *Barred Galaxies*, IAU Colloq. **157**, ed. R. Buta, D. A. Crocker & B. G. Elmegreen (ASP Conf series 91), p. 309
- Athanassoula, E. 2003, *MNRAS*, **341**, 1179
- Binney, J. & Tremaine, S. 1987, *Galactic Dynamics* (Princeton: Princeton University Press)
- Chandrasekhar, S. 1943, *ApJ*, **97**, 255
- Debattista, V. P. & Sellwood, J. A. 1998, *ApJ*, **493**, L5
- Debattista, V. P. & Sellwood, J. A. 2000, *ApJ*, **543**, 704
- Hernquist, L. 1990, *ApJ*, **356**, 359
- Hernquist, L. & Weinberg, M. D. 1992, *ApJ*, **400**, 80
- Holley-Bockelmann, K., Weinberg, M. & Katz, N. 2003, *astro-ph/0306374*
- Kalnajs, A. J. 1977, *ApJ*, **212**, 637
- Lin, D. N. C. & Tremaine, S. 1983, *ApJ*, **264**, 364
- Lynden-Bell, D. 1979, *MNRAS*, **187**, 101
- Lynden-Bell, D. & Kalnajs, A. J. 1972, *MNRAS*, **157**, 1

- Mulder, W. A. 1983, *A&A*, **117**, 9  
 Navarro, J. F., Frenk, C. S. & White, S. D. M. 1996, *ApJ*, **462**, 563  
 O'Neill, J. K. & Dubinski, J. 2003, *MNRAS*, **346**, 251  
 Sellwood, J. A. 1980, *A&A*, **89**, 296  
 Sellwood, J. A. 2003, *ApJ*, **587**, 638  
 Tremaine, S. & Weinberg, M. D. 1984, *MNRAS*, **209**, 729 (TW84)  
 Valenzuela, O. & Klypin, A. 2003, *MNRAS*, **345**, 406  
 Weinberg, M. D. 1985, *MNRAS*, **213**, 451  
 Weinberg, M. D. 2004, *astro-ph/0404169*  
 Weinberg, M. D. & Katz, N. 2002, *ApJ*, **580**, 627

#### APPENDIX

The NFW (Navarro, Frenk & White 1996) halo density profile is

$$\rho_{\text{NFW}} = \frac{\rho_s r_s^3}{r(r + r_s)^2}, \quad (1)$$

where  $\rho_s$  is a scale density and  $r_s$  is a scale length. Edington's formula (Binney & Tremaine 1987, eq. 4-140b) readily yields an isotropic distribution function that is positive everywhere.

Note that the NFW profile has a more slowly declining outer density gradient than does the Hernquist profile (eq. 3), but is otherwise closely similar. The density and potential when  $r < r_s$  are almost the same, while the logarithmic mass divergence of NFW profiles is both numerically inconvenient and physically unimportant – the extra mass at large radii has such low orbital frequencies and feels such a weak perturbing field from the distant quadrupole that its contribution to the total torque must be negligible.

Since Figure 9 is to be compared with Fig. 1(a) in Weinberg (2004), I have adopted his units for this case only. Considering his model halo to have a NFW concentration parameter of 15, Weinberg chooses  $15r_s$  to be his length unit, the mass interior to this radius as his mass unit, and he also sets Newton's constant  $G = 1$ . He chooses a large, strong, heavy bar, with semi-major axis equal to  $r_s = 1/15$ , axis ratios  $a : b : c = 1 : 0.2 : 0.05$ , and a mass equal to half the halo mass interior to this radius, or 0.053 of the virial mass. He chooses the initial pattern speed of the bar so as to place corotation at the bar end, which works out to be 18.9 in his units, and grows the perturbing potential as  $f(t) = [1 + \text{erf}(4t - 2)]/2$ .